LA-UR-21-22207 (Accepted Manuscript)

Prospects and challenges of colloidal quantum dot laser diodes

Jung, Heeyoung
Ahn, Namyoung
Klimov, Victor Ivanovich

To be published in: Nature Photonics

DOI to publisher's version: 10.1038/s41566-021-00827-6

Permalink to record: http://permalink.lanl.gov/object/view?what=info:lanl-repo/lareport/LA-UR-21-22207

Prospects and Challenges of Colloidal Quantum Dot Laser Diodes

Heeyoung Jung, Namyoung Ahn, Victor I. Klimov*

Chemistry Division, Los Alamos National Laboratory, Los Alamos, New Mexico 87545, USA

**e-mail: klimov@lanl.gov*

Colloidal quantum dots (QDs) combine superior light-emission characteristics of quantum-confined semiconductors with chemical flexibility of molecular systems. These properties could, in principle, enable solution processable laser diodes with an ultrawide range of accessible colours. However, the realization of such devices has been hampered by fast optical gain decay due to nonradiative Auger recombination and poor stability of QD solids at high current densities required for the lasing regime. Recently, these problems have been resolved, which resulted in the development of electrically pumped optical-gain devices operating at ultrahigh current densities up to ~1000 A cm^{-2}. The next step is the realization of a QD laser diode (QLD). Here, we assess the status of the QD lasing field, examine the remaining challenges on a path to a QLD, and discuss practical strategies for attaining electrically pumped QD lasing.

After first demonstrations of stimulated emission from GaAs p-n junctions in the early 1960s[1,2], the semiconductor-laser technology has experienced tremendous growth and expanded its reach into numerous fields from consumer electronics and broadband telecommunication to scientific research and space exploration. Modern semiconductor lasers comprise one or multiple two-dimensional (2D) semiconductor layers, or 'quantum wells,' incorporated into a diode-like charge-injection architecture[3]. These devices, often referred to as 'laser diodes,' are based most commonly on binary, ternary or quaternary combinations of III-V semiconductors fabricated via vacuum-based layer-by-layer deposition[4]. Further expansion of the laser diode technology into new areas of applications could be facilitated by the availability of electrically pumped lasers based on

solution processable materials. Such devices would simplify implementation of on-chip optical interconnects[5,6] and integrated photonic circuits[7,8]. They would also be of great practical utility in wearable technologies[9], lab-on-a-chip devices[10], and advanced medical imaging and diagnostics[11]. An attractive materials system for realizing solution-processable laser diodes is colloidal semiconductor nanocrystals[12-15]. These structures can be fabricated with near-atomic precision as quasi-spherical particles or 'quantum dots' (QDs)[16,17], elongated nanorods[18,19], branched tetrapods[20], and quantum-well-like nanoplatelets[21,22]. They comprise a crystalline inorganic semiconductor core overcoated with organic ligand molecules. Due to simultaneous presence of inorganic and organic constituents, colloidal nanocrystals combine chemical processibility of molecular systems with well-understood electronic and optical behaviours of zero-dimensional (0D) semiconductors. In addition, they offer unmatched flexibility for controlling their properties through means such as quantum confinement, hetero-structuring, controlled surface modifications, and incorporation of 'functional' defects[17,18,23,24].

Several latest developments indicate a considerable potential of colloidal nanocrystals as optical gain media capable of operating under both optical an electrical pumping. These include recent demonstration of optically pumped continuous wave (cw) colloidal QD lasing[25], the realization of optical gain with electrically pumped QDs[26], the development of on-chip-integrated optically-excited QD lasers[27], and the demonstration of dual-function devices operating as an optically pumped laser and an electrically excited light-emitting diode (LED)[28].

The purpose of this Review is to assess the status of the field of colloidal QD lasers with special attention to challenges related to the realization of lasing with electrical pumping. Specific subjects include mechanisms for optical gain and competing processes, the realization of high-current density LEDs for achieving population inversion, practical architectures for integrating optical

resonators into LEDs, and strategies for implementing a complete device capable of operating as an electrically pumped laser diode.

Fundamentals of colloidal QD lasing

QD electronic states. In colloidal QDs carrier motion is restricted in all three dimensions, which corresponds to the regime of 0D confinement. As a result of spatial constraints imposed on electronic wavefunctions, QDs exhibit discrete electronic states whose energy depend on particle dimensions. In spherical QDs, electronic states are usually labelled according to their principle (n = 1, 2, 3, …) and orbital (L = 1, 2, 3, …) quantum numbers and denoted as nL, where L is presented as a letter using an atomic-like progression S, P, D, etc. If arranged in the order of increasing energy, the three lowest states are 1S, 1P, and 1D (Fig. 1a).

In spherical QDs, a bandgap (E_g) can be approximated as a sum of a bulk bandgap ($E_{g,0}$) and the size-dependent 'confinement' energies of the band-edge electron ($1S_e$) and hole ($1S_h$) states (Fig. 1a):

$$E_g = E_{g,0} + E_{e,1,0} + E_{h,1,0} = E_{g,0} + \frac{\hbar^2\pi^2}{2m_eR^2} + \frac{\hbar^2\pi^2}{2m_hR^2} = E_{g,0} + \frac{\hbar^2\pi^2}{2m_{eh}R^2}, \quad (1)$$

where m_e and m_h are the effective electron and hole masses, and $m_{eh} = m_em_h/(m_e + m_h)$. Equation (1) indicates that the QD bandgap increases as R^{-2} with decreasing QD size. The correction to the bulk bandgap arising from quantum confinement ($E_{conf} = E_g - E_{g,0} \propto R^{-2}$) can reach hundreds of meV in sufficiently small particles. This underlies one of the key properties of the QDs, which is a size-controllable emission wavelength. As illustrated in Fig. 1b, employing this effect, it is possible to tune QD emission across infrared, visible, and ultraviolet spectral ranges using size-

varied QDs of selected II-VI, III-V, and IV-VI semiconductors[17,29-38]. This continuous spectral tunability is highly beneficial for applications in light-emission technologies and, especially, lasing as it can help fill spectral gaps not accessible with traditional semiconductor lasers.

Optical gain mechanism. In addition to the size-tunable bandgap, a distinctive feature of QDs is a wide separation between their atomic-like levels (Fig. 1a). This inhibits thermal depopulation of the band-edge states and thereby reduces optical gain threshold and makes it less sensitive to changes in temperature[15,39-41], the factors that motivated the development of QD lasers.

The processes of light amplification, which underlies lasing, relies on the effect of stimulated emission. Stimulated emission represents a response of a material to an incident photon when instead of absorbing it, the material generates the second photon whose characteristics are identical to those of the original one. Light amplification, or 'optical gain', occurs when stimulated emission overwhelms optical absorption, which corresponds to the situation when the number of excited atoms or molecules, that emit light, is greater than the number of light-absorbing species remaining in the ground state. This condition is commonly referred to as 'population inversion'.

Key feature of optical gain in a QD medium can be understood by analysing interplay between light absorption and stimulated emission in a system comprising $1S_e$ and $1S_h$ levels whose degeneracies (g_e and g_h, respectively) are equal to 2 due to two possible directions of a carrier spin (Fig. 1c). In a QD ground state, the valence band (VB) level contains two electrons each of which can absorb an incident photon (Fig. 1c, left). Excitation of a VB electron to the conduction band (CB) creates a single electron-hole (e-h) pair or an 'exciton'. This state corresponds to QD 'optical transparency' as stimulated emission by the CB electron is exactly compensated by light absorption arising from the VB electron (Fig. 1c, middle). In order to enact optical gain, one has to excite the second electron to the CB. In this situation, the absorption is completely eliminated

and the QD starts to amplify light (Fig. 1c, right). This implies that when $g_e = g_h = 2$ optical gain originates from the QDs that contain two-e-h-pair states or 'biexcitons'[12]. This further suggests that the gain threshold is realized when an average per-dot excitonic occupancy, $\langle N \rangle$, approaches 1 (refs 12,42); and when $\langle N \rangle$ is greater than 1, the QD system becomes 'inverted'.

In order to compute the gain threshold, $\langle N_{th,gain} \rangle$, for QDs whose degeneracies are distinct from 2, one can use a general gain-threshold condition, $\langle n_{1S,e} \rangle + \langle n_{1S,h} \rangle = 1$, where $\langle n_{1S,e} \rangle = \langle N \rangle / g_e$ and $\langle n_{1S,h} \rangle = \langle N \rangle / g_h$ are average single-state occupation factors calculated assuming that all carriers reside in the band-edge states[15] (this assumption is valid when $\langle N \rangle \leq g_{e,h}$ and the effect of thermal excitation into higher-energy states is negligible). Based on these expressions, $\langle N_{th,gain} \rangle = g_e g_h / (g_e + g_h)$. As expected, this yields $\langle N_{th,gain} \rangle = 1$ for the QDs with two-fold degenerate $1S_e$ and $1S_h$ levels, which describes fairly accurately CdSe-based QDs, especially in the case of asymmetrically strained structures with a large light-heavy hole splitting[25,26]. If $g_{e,h} > 2$, the gain threshold becomes greater than one exciton per dot. This, in particular, represents one of the complications for realizing lasing with infrared (IR) emitting PbS or PbSe QDs for which $g_e = g_h = 8$ and, as a result, $\langle N_{th,gain} \rangle$ is increased to 4 (ref. 43).

Several approaches have been explored in the literature for reducing the gain threshold to values below those defined by intrinsic degeneracies of the QD band-edge levels. One of them entails the use of 'giant' exciton-exciton repulsion in specially engineered QDs for displacing the absorbing transition associated with an exciton state versus its emitting transition[44]. Another method exploits QD doping (or charging) with permanent electrons for supressing ground state absorption competing with stimulated emission[45]. This approach was implemented using electrochemical[46],

photochemical[45,47], and electrical[48] injection of electrons into the QDs, as well as chemical doping[49].

Auger recombination and its implications for QD lasing. Multiexcitonic nature of light amplification in QDs greatly complicates the realization of lasing because of very fast optical gain decay due to nonradiative Auger recombination. In this process, an e-h recombination energy is not emitted as a photon but instead is transferred to a third carrier (an electron or a hole) residing in the same dot (Fig. 1d, right). As a result, this process directly competes with stimulated emission (Fig. 1d, left) and, if it is fast enough, it can completely suppress lasing.

In bulk semiconductors, the rates of Auger decay are low due to constraints associated with translational momentum conservation[50]. In 0D QDs, the momentum conservation is relaxed, which greatly enhances Auger decay rates[51] and leads to extremely short (ps to sub-ns timescales) biexciton Auger lifetimes ($\tau_{A,XX}$)[52,53].

Already early studies of Auger decay in colloidal CdSe QDs revealed that $\tau_{A,XX}$ exhibits linear scaling with particle volume (V_{QD})[52]. This trend, known as 'V-scaling' is very general and can be described by $\tau_{A,XX} = \chi V$, where χ is a composition-independent constant of ~1 ps nm^{-3} (refs 24,53). Based on the 'universal' V-scaling, $\tau_{A,XX}$ is from ~4 to ~270 ps for R = 1−4 nm, which is a size range typical of colloidal QDs. The Auger time constants are much shorter than a biexciton radiative lifetime ($\tau_{r,XX}$), indicating strong quenching of biexciton emission due to the Auger effect. For example, in CdSe QDs, $\tau_{r,XX}$ is ~5 ns (~4 times shorter than $\tau_{r,X}$ = 20 ns for excitons[54,55]), which yields the biexciton emission quantum efficiency (q_{XX}) of ~0.1 to ~5%, depending on QD size. These values are estimated from $q_{XX} \approx \tau_{A,XX}/\tau_{r,XX}$, taking into consideration that $\tau_{A,XX} \ll \tau_{r,XX}$ and hence the overall biexciton lifetime (τ_{XX}) is close to $\tau_{A,XX}$. A very low

emissivity of biexcitons creates a serious problem for lasing in QDs as stimulated emission from biexciton states underlies optical gain in these materials.

An obvious complication arising from Auger recombination is a dramatic shortening of the optical gain lifetime (τ_{gain}) as it is determined by τ_{XX}. This also leads to the increase in the optical gain and lasing thresholds, which is especially significant in the case of cw optical and direct-current (d.c.) electrical pumping[15]. Yet another less apparent consequence of Auger decay is its influence on a minimal (critical) QD volume fraction ($\xi = \rho_{QD} V_{QD}$) required for the lasing effect (here ρ_{QD} is the QD concentration)[12,15]. Indeed, for lasing to occur, the rate of stimulation emission (r_{SE}) must exceed that of optical gain decay (r_{gain})[12]. The former of these quantities is proportional to ξ ($r_{SE} = \xi / \tau_0$; τ_0 is a time constant defined by the details of a QD-optical-cavity system[42]) and the later scales inversely with $\tau_{A,XX}$ ($r_{gain} = 1/\tau_{gain} = (\theta \tau_{A,XX})^{-1}$; θ is a constant of around 1 or less[56]). As a result, the critical QD volume fraction (ξ_{crit}), defined by condition $r_{SE} = r_{gain}$, can be found from $\xi / \tau_0 = (\theta \tau_{A,XX})^{-1}$. This equation yields $\xi_{crit} = \theta^{-1}(\tau_0 / \tau_{A,XX})$. If we describe $\tau_{A,XX}$ using a V-scaling, $\xi_{crit} = \theta^{-1} \chi^{-1} (\tau_0 / V_{QD}) \propto R^{-3}$. This expression indicates that the QD volume fraction needed for achieving lasing quickly increases with decreasing dot size. This is a direct consequence of the increasing rate of Auger decay, which requires faster stimulated emission for achieving lasing.

A direct connection between QD gain and biexciton states was originally revealed by studies of refs 12,52. These works also established the existence of ξ_{crit} which motivated the authors of ref. 12 to use in their optical gain experiments close-packed QD films with ξ>15%, which exceeded ξ_{crit} (estimated as 0.2 – 2%; refs 12,42) by a considerable margin. This was a critical distinction from prior studies utilizing low-density QD solution samples. Another important element of that work was the use of short-pulse pumping (τ_p = 100 fs), which allowed for quickly populating QDs

with biexcitons before the onset of Auger decay. The use of dense QD solids along with ultrafast pumping were two key ingredients of the first practical demonstration of amplified spontaneous emission (ASE) with colloidal QDs[12].

Following these proof-of-principle experiments, a true lasing action was soon realized using QD solids coupled to various types of optical cavities[57-59]. The lasing studies were also extended to shape-controlled CdSe-based nanocrystals (e.g., nanorods[60,61] and nanoplatelets[62,63]) and structures of other compositons including perovskites[64]. However, despite a wide variety of demonstrated nanocrystal-based optical gain materials and lasing schemes, the main principles of nanocrystal-based lasing devices have largely remained the same as in the original demonstration of ASE[12]. In particular, the majority of the conducted studies have used high-intensity, sub-ps optical pulses for QD pumping, which greatly limits practical utility of the realized devices.

A necessary condition for turning colloidal QD lasing into a viable technology is the development of effective approaches for achieving lasing with low-intensity cw optical and electrical excitation. In the follow-up sections, we will discuss the challenges on the path to this objective, and existing and prospective approaches for their solution. The focus in this discussion will be on methods for realizing electrically pumped devices, that is, quantum dot laser diodes (QLDs).

Principles of colloidal QD laser diodes

From a QD-LED to a QLD. More than two decades of research into QD-based electroluminescent (EL) devices or QD-LEDs have produced impressive advances in their performance[24,65]. State-of-the-art devices exhibit high external quantum efficiencies (EQEs) of ~20% (ref. 66), which is a limit imposed by a light extraction coefficient from a semiconductor medium (EQE is defined as a ratio of the total number of photons emitted by a device and the

number of injected e-h pairs). Specially optimized LEDs also reached extremely high brightness levels of the order of 10^5–10^6 cd m^{-2} (refs 67-69).

As depicted in Fig. 2a, a typical QD-LED features a p-i-n architecture wherein a thin, 1–2 monolayer (ML) QD film is sandwiched between an n-type electron and a p-type hole transport layer (ETL and HTL, respectively)[24,65,70]. This design alleviates the problem of poor charge conductance of a QD solid and facilitates injection of both types of carriers under forward bias and minimizes device current under reverse bias. A QLD can be thought of as a standard LED, which contains either an internal (integrated) or external optical cavity required for circulating light through a QD optical gain medium (Fig. 2b). One challenge in realizing this structure is effective mitigation of damping of cavity modes due to optical losses in various charge conducting layers of an LED device stack. A further potential problem is disruption of charge injection pathways caused by the integrated optical resonator. A final complication is the need for extremely high current densities (j) required for achieving optical gain values that are sufficient for compensating optical losses in the laser cavity.

Excitation and relaxation pathways in a QLD. First, we need to understand a distinction between excitation/relaxation pathways in a QLD versus a standard LED. In a traditional LED, a QD is circulated between a ground (unexcited) and a single-exciton state (Fig. 2c, excitation/relaxation cycle highlighted by blue shading). The realization of a QLD, on the other hand, requires the involvement of a gain-active biexciton state (Fig. 2c, excitation/relaxation cycle highlighted by red shading). The arising problem is the need for considerably higher current densities, as in this case, charge carrier inflow must outpace nonradiative biexciton decay via the Auger process. A related challenge arises from potential charge imbalance common in the regime

of high j. The development of such imbalance can lead to generation of 'undesired' charged states at the expense of 'desired' neutral biexcitons.

Let us first consider the charge-imbalance problem. In the regime of ideal ('balanced') injection, the emitting exciton state is produced via two ordered steps when injection of one charge (typically, an electron[70]) is followed by the injection of a charge of the opposite sign (Fig. 2c, blue and black arrows, respectively). If, for example, the injection rate for the electron (g_e) is much greater than that for the hole (g_h), this leads to 'imbalanced' injection which generates charged excitons (trions) instead of neutral excitons. This excitation pathway is undesired in LEDs, as it opens a nonradiative decay channel arising from Auger recombination[67,70].

While charge imbalance is a common phenomenon at large current densities, in the case of moderate j (for example, close to the EL turn-on), QD LEDs typically do not exhibit signatures of imbalanced injection. As was suggested in ref. 26, this self-maintained charge balance can be ascribed to the effect of Coulomb interactions. In particular, if a QD contains a charge of a certain sign, this favours the injection of a charge of an opposite sign as Coulomb attraction reduces the injection barrier. On the other hand, the injection of the charge of the same sign is inhibited due to an additional potential barrier created by Coulomb repulsion.

This phenomenon can be described in more quantitative terms using a simple model of a charged sphere. The electrostatic (Coulomb) energy a 'QD-sphere' containing a single electron is given by $E_c = E_{c,1} = (2C)^{-1}e^2$, where e is the elementary charge, C is the effective QD capacitance defined by its radius and a dielectric constant of a surrounding medium (ε): $C \propto \varepsilon R$. If we add a hole to this negatively charged dot, the resulting state will be a charge-neutral exciton with $E_{c,0} = 0$. Hence, hole addition represents a downhill process accompanied by the release of energy $\Delta E_{eh} = E_{c,0} - E_{c,1} = -E_{c,1}$ (Fig. 2c, black solid arrow within the 'blue cycle'). In contrast, if one attempts to add

an electron, the electrostatic energy increases by $\Delta E_{ee} = E_{c,2} - E_{c,1} = 3E_{c,1}$, implying that this is an energy consuming uphill process (Fig. 2c, blue dashed arrow). The energy difference between the two final states (neutral-exciton and two-electron states) is $4E_{c,1}$. Even in large-size QDs with R of 4−5 nm, it can reach very large values of more than 200 meV. This energy acts as a driving force, which favours injection steps leading to QD neutralization versus those increasing the QD charge. This allows us to assume that $g_e = g_h = g$ and, hence, excitation of a QD by an electric current occurs via injection of charge neutral e-h pairs, which mimics the case of optical pumping. Based on this assumption, we can model a QLD regime using a three-state optical gain description previously developed for the case of optical excitation[42].

Optical gain and lasing thresholds in the case of electrical excitations. The three-state model, depicted in Fig. 3a, takes into consideration the ground, $|0\rangle$, single exciton, $|X\rangle$, and biexciton, $|XX\rangle$, states, which occur with probabilities P_0, P_X , and P_{XX}, respectively. Here, we assume that the exciton emission energy ($|X\rangle-|0\rangle$ transition) is the same as its absorption energy ($|X\rangle-|XX\rangle$ transition). In general, however, these two energies differ by the exciton-exciton interaction energy (Δ_{XX})[44]. Normally, Δ_{XX} is smaller than the inhomogeneous emission linewidth of a QD ensemble sample and, therefore, the influence of the exciton-exciton interaction on optical gain is insignificant. However, in specially engineered type-II hetero-QDs, that feature spatial separation between an electron and a hole wavefunction, Δ_{XX} can reach 'giant' values of ~100 meV, which has been exploited for realizing 'single-exciton' optical gain[44].

To describe the regime of d.c. electrical pumping, we assume that the three-state system in Fig. 3a is excited with a constant per-dot rate g, which induces the upward $|0\rangle-|X\rangle$ and $|X\rangle-|XX\rangle$ transitions. In the pre-lasing regime, the downward transitions between the same states occur due to spontaneous decay of the exciton and the biexciton with rates $r_X = 1/\tau_X$ and $r_{XX} = 1/\tau_{XX}$,

respectively. Under steady-state conditions, the upward and downward excitation flows balance each other, that is, $P_{XX}/\tau_{XX} = gP_X$ and $P_X/\tau_X = gP_0$. By combining these two rate equations with the normalization condition ($P_0 + P_X + P_{XX} = 1$), we obtain $P_0 = 1/D$, $P_X = \tilde{g}/D$, and $P_{XX} = \tilde{g}^2/(\beta D)$, where $\tilde{g} = g\tau_X$, $\beta = \tau_X/\tau_{XX}$, and $D = 1 + \tilde{g} + \beta^{-1}\tilde{g}^2$.

Using the above solutions, we can derive the dependence of optical gain on g and then quantify optical gain and lasing thresholds ($g_{th,gain}$ and $g_{th,las}$, respectively). Since single excitons are gain-neutral (Fig. 3a), net optical gain (G) is proportional to $P_{inv} = P_{XX} - P_0$, that is, $G = G_0P_{inv}$, where P_{inv} is per-dot population inversion, and G_0 is the maximal (saturated) gain, realized when every dot contains a biexciton[42]. Optical gain threshold corresponds to $P_{inv} = 0$ or $P_{XX} = P_0$. Applying this condition to the rate equations derived earlier, we obtain $g_{th,gain} = (\tau_{XX}\tau_X)^{-½} = (r_X r_{XX})^{½}$. This expression indicates a direct connection of $g_{th,gain}$ to the exciton and biexciton decay rates. The dependence of the optical gain threshold on r_{XX} is especially harmful, as very fast biexciton Auger decay can raise $g_{th,gain}$ to prohibitively high levels, inaccessible in QD-LEDs.

Auger decay represents even a more serious obstacle for achieving lasing. In this case, the required excitation rate is higher than $g_{th,gain}$, as it should be sufficient for maintaining nonzero steady-state gain whose magnitude is high enough to compensate cavity losses. To estimate the lasing threshold, we assume that the attainment of the lasing regime requires $G = G_{½} = 0.5G_0$ or $P_{inv} = 0.5$. Based on the rate equations, the corresponding excitation rate ($g_{½}$) is: $g_{½} = (2\tau_{XX})^{-1}[1 + (1 + 12\tau_{XX}/\tau_X)^{1/2}]$ or $g_{½} \approx 1/\tau_{A,XX}$, if $\tau_{A,XX} \ll \tau_{r,XX}$. We can further relate $g_{½}$ to $g_{th,gain}$ by $g_{½} = \sqrt{\beta}\, g_{th,gain} \approx \sqrt{\tau_X/\tau_{A,XX}}\, g_{th,gain}$. Since in standard QDs, τ_X is much longer than $\tau_{A,XX}$, $g_{½}$ is considerably higher than $g_{th,gain}$. For example, for mid-size CdSe QDs with R = 3 nm, $\tau_{A,XX}$ is ~110 ps, which

yields β of ~180. This indicates that the lasing thresholds (estimated as $g_{½}$) is a factor of ~13 higher than the gain threshold, which is the direct consequence of fast Auger recombination.

To express optical gain and lasing thresholds in terms of a current density, we present the generation rate as $g = \sigma_e(j/e)$, where σ_e is a QD electrical cross-section[15]. In order to estimate σ_e, we consider a typical LED architecture, wherein QDs are incorporated as a single-ML film. Due to a QD organic capping layer and residual unbound ligands, the areal semiconductor filling factor (f) in a film is typically around 0.5 – 0.6 (ref. 15). Since organic molecules occupying the interdot space are nonconducting, the device current flows preferentially through QD semiconductor cores (Fig. 3b). Due to this natural 'current focusing,' the QD electrical cross-section is increased compared to its geometrical cross-section ($\sigma_g = \pi R^2$) by a factor of $1/f$, that is, $\sigma_e = \sigma_g/f$.

Using the derived connection between g and j, we can re-write the expressions for $g_{th,gain}$ and $g_{½}$ in terms of corresponding current densities:

$$j_{\mathrm{th,gain}} = \frac{ef}{\sigma_g\sqrt{\tau_X\tau_{XX}}} \qquad (2)$$

and

$$j_{1/2} = \frac{ef\left(1+\sqrt{1+12\tau_{XX}/\tau_X}\right)}{2\sigma_g\tau_{XX}} \qquad (3)$$

Applying equations (2) and (3) to the case of standard CdSe QDs with R = 3 nm used in our earlier estimations and assuming f = 0.5, we obtain $j_{th,gain}$ = 0.19 kA cm^{-2} and $j_{½}$ = 2.5 kA cm^{-2}. Both of these values are orders of magnitude higher than maximal current densities (j_{max}) realized in

standard QD-LEDs, for which j_{max} is typically limited by ~1 A cm^{-2} due to device breakdown[66,68,69].

It is instructive to evaluate probabilities P_i (i = 0, X, XX) realized in a standard LED in the range of maximal (pre-breakdown) currents. Assuming j = 1 A cm^{-2} and R = 3 nm, and using the rate equations, derived earlier, we obtain $P_0 \approx 0.93$, $P_1 \approx 0.07$, and $P_2 \approx 3\times10^{-5}$. This suggests that in the standard LED, even at the maximal currents densities, most of the QDs remains in the ground state, and only a small portion of them (~7%) is populated with single excitons. The fraction of dots containing biexcitons is vanishingly small (~0.003%), implying that the operational cycle stays limited to the ground and single-exciton states and never extends to the biexciton state (Fig. 2c, 'blue cycle').

If we conduct similar estimations for $j = j_{½}$, which approximately corresponds to the lasing threshold, we obtain $P_0 \approx 3\times10^{-3}$ and $P_1 = P_2 \approx 0.5$. This indicates that during a QLD operational cycle, a QD is circulated primarily between the single-exciton and biexciton states (Fig. 2c, 'red cycle'). This is a sharp distinction from the regime of a standard LED, suggesting that the realization of a QLD cannot rely on traditional QD-LED schemes but requires novel approaches to both QD emitters and the EL architecture.

Realization of optical gain with electrical excitation

Control of electrical cross-section and Auger recombination. A potential approach to reducing threshold currents required to attain optical gain and lasing regimes is the use of large-volume hetero-QDs containing a small, quantum-confined 'emitting' core enclosed into a thick shell of a wider-gap semiconductor. This can allow for boosting both the QD electrical cross-section and the

Auger lifetime and, importantly, do so without losing the benefits of 0D confinement and retaining the ability to tune the emission wavelength by varying the size of the quantum-confined core. This capability would be lost in the case of large-size mono-component (core-only) nanocrystals that would exhibit bulk-like properties.

QD hetero-structuring has been previously explored in the context of lasing using so-called 'giant' CdSe/CdS QDs that exhibited the expected improvements in optical gain properties[71,72] and allowed, in particular, for a recent demonstration of optically excited cw lasing[25]. Further improvements in the lasing performance have been achieved with a new generation of 'giant' dots that feature a small CdSe core enclosed into a continuously graded (cg) shell of a $Cd_xZn_{1-x}Se$ alloy (Fig. 3c)[26,47]. This approach leads to smoothing of the electron and hole confinement potential, which allows for strong suppression of Auger decay in both 0D QDs[73] as well as traditional 2D quantum wells[74]. The reduction of Auger rates occurs due to the reduced strength of the intra-band transition involved in the dissipation of the e-h recombination energy[73]. As a result, cg-QDs exhibit long Auger lifetimes ($\tau_{A,XX}$ > 2 ns; refs 26,47] and high biexciton emission efficiencies of more than 40%, which is in sharp contrast to q_{XX} of less than 3% for standard CdSe QDs with a similar bandgap[26,47].

Excellent optical gain properties of $CdSe/Cd_xZn_{1-x}Se$ cg-QDs have underlain several recent advances in the QD lasing including the realization of low-threshold dual-band 1S and 1P lasing[26] (Fig. 3d) as well as the demonstrations of 'zero-threshold' optical gain[45] and sub-single-exciton lasing[47] with charged QDs. Further, the cg-QDs have also shown good performance as EL materials and, in particular, allowed for realizing high-brightness LEDs whose luminance exceeded 300,000 cd m^{-2} (ref. 67). These dots were also employed to realize optical gain in high-

current-density LEDs[26] and to demonstrate dual-function devices that operated as both an optically excited laser and a standard electrically pumped LED[28].

So far, most of the efforts to control Auger recombination have focused on visible-light-emitting II-VI QDs. The next step is to transfer the developed approaches to QDs of IR emitting materials. The availability of effective approaches for suppressing Auger decay would be especially beneficial in the case of narrow-gap PbSe(S)-based QDs. As discussed earlier, due to a high degeneracy of their band-edge states, activation of optical gain requires high-order multiexcitons with $N > 4$. This leads to extremely short optical-gain lifetimes due to fast scaling of Auger rates with exciton multiplicity[75], which greatly complicates the realization of lasing with cw optical and d.c. electrical excitation.

Manipulation of charge injection. As discussed in the previous section, realization of electrically pumped lasing requires exceptionally high current densities that are orders of magnitude higher than those previously attained with standard QD-LEDs. Achieving this regime requires injection architectures that can support j of tens and hundreds of A per cm^2 without device damage. The other is to ensure that device characteristics and, in particular, the EL efficiency do not degrade (reversibly or irreversibly) at high j.

One process, which has a deleterious effect on both the stability and the performance of QD-LEDs is Auger recombination[24,67,68,70]. As was stated earlier, in this process the e-h recombination energy is released in the form of a kinetic energy of a third carrier, which leads to so-called 'Auger heating'[76] and thereby accelerates device degradation. Auger recombination has been also invoked to explain a progressive (reversible) decrease of the LED EQE ('EQE droop') with increasing current density observed for both traditional III-V quantum well-based LEDs[77] as well as QD LEDs (Fig. 4a)[67,70]. In the case of colloidal QDs, this phenomenon has been ascribed to increasing

imbalance between electron and hole injection currents, which leads to accumulation of long-lived uncompensated charges in the QDs. The presence of such charges triggers a nonradiative Auger recombination and, as a result, leads to an EQE fall-off (Fig. 4a).

In standard QD LEDs, operating in a sub-single exciton regime, Auger recombination can be circumvented by properly balancing electron and hole injections (see below). However, it is unavoidable in optical gain devices (that is, amplifiers and lasers) as their operation relies on stimulated emission from biexcitons and other multi-carrier species. This re-emphasizes the importance of effective control of Auger recombination for the realization of QLDs. As was discussed earlier, this can help extend an optical gain lifetime and thereby lower the lasing threshold. Simultaneously, this would allow for enhancing the EL efficiency (due to reduced nonradiative carrier losses) and improving device stability (due to suppressed Auger heating).

Previously, the benefits of QDs with suppressed Auger recombination have been exploited in the context of the development of high-brightness devices for application in areas such as daylight displays, outdoor signage, and see-through screens[67,78]. A pronounced difference in LED performance of QDs with varied degrees of Auger-decay suppression is illustrated in Fig. 4b. This plot displays the dependence of EQE on device brightness (L) for LEDs based on compositionally graded CdSe/$Cd_xZn_{1-x}Se$ cg-QDs and devices made of similarly sized 'ungraded' core/shell CdSe/$Cd_{0.7}Zn_{0.3}Se$ QDs[67]. Due to a 'smoothened' confinement potential, the graded structures exhibit a stronger suppression of Auger decay than standard core/shell QDs, which manifests, in particular, in a higher PL quantum yield of negative trions (~50% versus 18%; ref. 67). The inhibition of Auger recombination also leads to improved LED performance as indicated by the enhanced peak EQE and the reduced EQE droop (compare green squares and blue circles in Fig. 4b).

While ‘Auger-decay engineering’ helps improve EQE by increasing emissivity of charged species, further gains in the LED performance can be obtained by improving charge balance during device operation. This objective can be accomplished by either manipulating the structure of individual QDs or optimizing the device architecture. The first of these approaches is illustrated in Fig. 4b, which displays an EQE trace obtained for an LED made of modified cg-QDs, which in addition to a graded layer contain a final shell of wide-gap $ZnSe_ySe_{1-y}$ (red triangles; ref. 67). This additional barrier layer (‘B-layer’) selectively impedes electron injection and helps mitigate oversupply of electrons, a problem typical of an ‘inverted’ architecture often applied in high-performance LEDs, including devices in Fig. 4b. As a result of a combined effect of strong Auger-decay suppression (due to the cg-layer) and improved injection balance (due to the B-layer), the use of cg/B-QDs allowed for further EQE improvements versus ‘barrier-less’ cg-QDs (compare red triangles and blue circles in Fig. 4b). Importantly, this strategy resulted in virtually droop-free performance up to j of ~0.5 A cm^{-2}, which was key to demonstrating very high brightness levels of more than 300,000 cd m^{-2} (ref. 67).

Effective control of charge balance can also be achieved via device-level manipulation of charge injection. An inverted LED design commonly utilizes an inorganic ZnO ETL and an organic HTL made of, for example, 4,40-bis(N-carbazolyl)-1,10-biphenyl (CBP) or tris(4-carbazoyl-9-ylphenyl)amine) (TCTA)[26,67,68,79]. This allows for a good match of ETL and HTL work functions with, respectively, CB and VB edges of the QDs. However, the hybrid inorganic/organic approach leads to a considerable disparity between ETL and HTL charge-carrier mobilities. In particular, the electron mobility of solution-processed ZnO (ca. 10^{-3} to 10^{-2} cm^2 $V^{-1}s^{-1}$; ref. 79) is usually considerably higher than the hole mobility of organic HTLs ($<10^{-4}$ cm^2 $V^{-1}s^{-1}$; ref. 80). As a result, electron injection outpaces hole injection, which contributes to charge imbalance.

Demonstrated device-level strategies to correct this problem employed insertion of thin insulating layers[66,81] or energetic barrier layers[82] into an electron-injection path and/or inclusion of low-mobility additives into an ETL material[67]. The first of these methods was exploited in studies leading to the demonstration of record-high EQEs of ~20% (ref. 66). The second approach was used in the research into high-brightness LEDs where it was combined with QD-level engineering of Auger-decay and charge-injection barriers (Fig. 4b), as discussed earlier[67].

While being successfully applied in standard QD-LEDs, the methods that rely on deliberate suppression of charge injection and/or transport are not well suited for implementing QLDs. These approaches increase device resistivity and, as a result, boost Joule heating (see next sub-section). In this situation, the preferred methods for controlling charge balance are those that employ enhancement of hole injection instead of suppressing electron injection. This can be accomplished by, for example, doping an HTL for boosting its conductance[83], incorporating engineered interlayers for achieving an Ohmic-contact-like regime of hole injection[84], or manipulating a hole injection barrier at the QD surface by means of polar ligands with appropriately aligned electric dipoles[85,86].

Control of Joule heating. In addition to a deleterious role of Auger heating discussed in the previous section, the realization of QLDs is complicated by problems arising due to Joule (or ohmic) heating. In standard LEDs, wherein QDs are incorporated as a single monolayer, charges are transported via non-QD device components, while QDs serve purely as 'radiative-recombination centers.' In this case, Joule heating is primarily caused by poor conductivity of chemically processed charge transport layers (CTLs) and high contact resistance between adjacent components of a device stack. The situation, however, is different in QLDs that might employ not one but multiple QD monolayers for boosting modal gain to levels that are sufficient to compensate

for optical losses. Activation of such a thick gain medium would necessarily involve charge transport within a poorly conductive 'granular' QD solid, which thus will become an additional source of Joule heat.

Previous studies of QD-LEDs show that because of their high resistivity they tend to overheat by tens and even hundreds of degrees centigrade even at moderate current densities of a few A per cm^2 (ref. 69). The exposure of QDs to high temperatures can lead to the reduction of their emission efficiency due to defects caused by a mismatch in thermal expansion coefficients of the core and shell materials[69,87] and/or degradation of a surface passivation layer[88]. It can also trigger unwanted modifications in the QD internal structure due to uncontrolled ion exchange at core/shell interfaces and ionic diffusion within compositionally graded layers[89,90].

Device overheating has also a deleterious effect on other components of a QD-LED. In particular, it can cause thermal damage of organic HTLs[91] or their unwanted modification due to crystallization and/or intermixing[92]. In addition to affecting electrical conductance, these structural changes may increase the likelihood of electrical breakdown due to a declining dielectric strength[93]. Further, a high device temperature can cause delamination of a metal contact used as a top electrode[94].

One approach to tackle the problem of excess heat is to reduce the device resistivity using methods similar to those discussed earlier in the context of control of injection balance. In addition, in the case of a thick QD active layer, which might be required for boosting modal gain, the exchange of original long organic ligands for shorter species can help enhance electrical conductance and thereby reduce generation of Joule heat. Previously, this approach has been successfully applied in QD LEDs[68], field effect transistors[95], and solar cells[96].

The problem of excess heat has been also tacked by improving 'thermal management' in an EL device[26,69,97-99]. In particular, heat dissipation can be enhanced using a high thermal conductivity (k) substrate which acts as a 'heat sink.' For example, according to measurements of ref. 69, devices assembled on a sapphire substrate ($k = 25$ $Wm^{-1}K^{-1}$) exhibited a maximal 'pre-degradation' current density of ~3.9 A cm^{-2} versus ~2.5 A cm^{-2} for a glass substrate ($k = 1.1$ $Wm^{-1}K^{-1}$)[69]. Due to improved thermal management, the sapphire-based LEDs were able to achieve extremely high brightness levels of more than a million cd per m^2 (ref. 69).

Improved heat dissipation can also be obtained by spatially confining the injection area with the aid of miniature charge-injecting contacts and/or small charge-conducting apertures incorporated into insulating interlayers within a device stack[26,97-99]. These 'current-focusing' schemes allow one to increase the ratio of a 'heat-emitting' surface area and an active (heat-generating) volume and thereby impede heat buildup compared to a non-focusing LED operating at the same j. Recently, this approach was utilized to boost j to levels sufficient to achieve population inversion, which allowed for demonstrating for the first time optical amplification in an electrically pumped colloidal-QD device[26].

Experimental demonstrations of electrically excited optical gain. Optical gain devices realized in ref. 26 utilized 1D current focusing implemented with a narrow (70 − 100 μm) slit incorporated into a thin insulating LiF spacer separating an HTL and a QD layer. This design allowed for reaching high current densities of more than 10 A cm^{-2} while avoiding considerable device overheating. In particular, based on spectral shifts observed in EL, at $j = 12$ A cm^{-2}, the overheating of the active volume was within ~20 ºC.

In addition to current focusing, the studies of ref. 26 took advantage of excellent EL and optical gain properties of thick-shell compositionally graded CdSe/$Cd_xZn_{1-x}Se$-based cg-QDs. As was

discussed earlier, these dots exhibit large electrical cross-sections and long biexciton lifetimes, which lead to a fairly low, sub-10 A cm^{-2} optical gain thresholds. In particular, based on equation 2, the parameters of the cg-QDs used in ref. 26 ($\sigma_g \approx 3\times10^{-12}$ cm^2, $f = 0.5$, $\tau_X \approx 12$ ns, and $\tau_{A,XX} \approx$ 2.4 ns) should allow one to attain population inversion with j of ~7 A cm^{-2}. The conducted measurements were consistent with this estimation and indicated the crossover from absorption to gain at around 3−4 A cm^{-2}. Further, a quantitative analysis of EL spectra showed that at the maximal current density realized in the studied devices (~18 A cm^{-2}), the average per-dot occupancy was more than 3 excitons. This indicated that the developed LEDs were able to attain complete inversion of the 1S band-edge transition and even achieve a partial population of the 1P electron excited state.

Even higher excitation densities were recently realized by applying 2D focusing in combination with pulse electrical excitation (Fig. 5a)[99], which helped reduce heat accumulation due to periodic interjection of shot heating cycles with long cooling periods. The benefits of this approach are illustrated in Fig. 5b (right), which shows a comparison of the dependence of the EL peak energy on applied bias (V) for a non-focusing LED operating in the d.c. regime (black triangles) versus a current-focusing structure excited with 1-μs pulses at a 100-Hz repetition rate (red circles). In both cases, the EL shifts to lower energies with increasing V, which is a signature of the reduction of the QD bandgap due to increasing temperature[100]. Based on the shift magnitude, the active volume of a non-focusing device, excited by a d.c. bias, heats up by ΔT of ~210 ºC at V = 14 V. At this point, the device experiences a breakdown, which limits the maximal attainable current density to ~3 A cm^{-2} (Fig. 5b, left).

Due to suppressed heat accumulation, the pulsed, current-focusing LED shows virtually no overheating up to V of 12 V, which is the voltage that caused irreversible damage to the first device.

Even at V = 60 V, the overheating of the active region is limited by ~100 ºC (inferred from the shift of the EL spectrum; red circles in Fig. 5b, right). This allows for pushing j to unprecedented values of 1,090 A cm^{-2} without imparting damage to any of the device components. Extremely high excitation levels realized in these devices lead to a very unusual EL regime when the intensity of the above-band-edge emission originating from the 1P electrons (1P band) becomes comparable to that of the 1S band observed for standard LEDs (Fig. 5c). Based on the quantitative analysis of the 1S and 1P EL features (Fig. 5d), these devices allow for attaining excitation densities of ca. 7 excitons per dot on average, which corresponds to complete population inversion of not only the 1S but also the 1P transition. This result is of great significance as saturated 1P gain is considerably higher than the maximal 1S gain, which can help tackle optical losses in a practical QLD device. Further, a very large bandwidth of optical gain, spanning the 1S and the 1P transitions can be exploited for realizing multi-color lasing and, perhaps, 'white-light' lasing with a single QD system.

Integration of optical resonators

The studies discussed in the previous section demonstrate the feasibility of achieving an optical gain regime with electrically pumped QDs[26,99]. The next step is the integration of an optical resonator in a functional EL device. One can envision two types of cavity designs for realizing a QLD. In one, photons are circulated in the direction normal to the device layers. This type of a resonator ('vertical' surface emitting Fabry-Perot cavity) can be implemented, for example, using metal mirrors that can simultaneously serve as charge-injecting electrodes[101,102]. However, the presence of metal layers in a device stack increases optical losses and makes it more difficult to achieve lasing. The losses can be reduced using dielectric distributed Bragg reflectors

(DBRs)[103,104] . However, achieving high-reflectivity with a DBR approach requires a large number of interchanging dielectric layers. This increases a device serial resistance and thereby complicates the realization of high current densities required for a lasing regime.

An alternative to a vertical cavity is an 'in-plane' cavity which circulates photons in the direction along the device layers. In the case of standard semiconductor laser diodes, such cavities have been realized using a cleaved-facet approach, which leads to 'edge-emitting' devices[105,106]. This method however, cannot be applied to solution processed structures made of 'non-cleavable' materials. In this case, the realization of an in-plane Fabry-Perot cavity requires additional fabrication steps for integrating optical reflectors into device edges[107].

An in-plane cavity effect can be also obtained using a distributed feedback resonator (DFB)[108]. It can be implemented by introducing a periodic 1D or 2D corrugation in one or multiple device layers (Fig. 6a)[28,98,108]. Cavity resonances of a DFB structure are defined by the Bragg condition[109]. In the case of a 1D grating, it yields $\lambda_m = 2n_{\text{eff}}\Lambda m^{-1}$, where m is the Bragg diffraction order, λ_m is the corresponding resonant wavelength, Λ is the grating period, and n_{eff} is the effective refractive index. Using a DFB approach one can realize both edge- and surface-emitting lasing structures[98,110]. In the first type of devices, in-plane feedback is realized due to the first-order diffraction and, as a result, the lasing wavelength is defined by $\lambda_{1as} = 2n_{\text{eff}}\Lambda$ (ref. 110). In the second type of structures, optical feedback arises from the second-order diffraction, while light outcoupling in a vertical direction occurs due to the first diffraction order[28,111,112]. In this case, the lasing wavelength can be found from $\lambda_{1as} = n_{\text{eff}}\Lambda$. An advantage of the second-order DFB resonators versus first-order structures is that they utilize longer grating periods and, therefore, are more readily accessible with inexpensive, high-throughput fabrication techniques such as standard photolithography[28,113] or nanoimprint lithography[114].

Recently, it has been demonstrated that the second order DFB grating can be incorporated into a QD-LED-like device and enable lasing action under optical excitation[28]. The developed structures had an architecture of a typical 'inverted' LED and comprised an ITO cathode, a ZnO ETL, an emitting layer made of CdSe/$Cd_xZn_{1-x}Se$/$ZnSe_{0.5}S_{0.5}$/ZnS cg-QDs, and a TCTA HTL (Fig. 6a,b). A second-order DFB grating was engraved into the bottom electrode which was made of a mixture of ITO and SiO_2 (low-index ITO or L-ITO). The use of L-ITO allowed for increasing the reflective-index contrast at the QD/electrode interface and thereby improving optical mode confinement in the QD layer.

To enable electrical excitation of the device, the active medium was only ~50-nm thick, which corresponded to 3 QD MLs (Fig. 6b). Because of its small thickness, the QD region was only a small part of the entire device, which resulted in a fairly small mode confinement factor (Γ_{QD}). Based on an intensity profile of an in-plane transverse electric mode (TE_0, red line in Fig. 6c), Γ_{QD} was 23%. Correspondingly, the maximal effective (modal) gain ($G_{m,0}$) was only a small fraction of saturated gain of a close-packed QD solid. Based on variable-stripe measurements of ASE of cg-QD films, $G_0 \approx 200$ cm^{-1}, which yields $G_{m,0} = \Gamma_{QD}G_0 \approx 46$ cm^{-1}.

To evaluate whether the estimated modal gain is sufficient to overcome optical losses, we calculate an effective absorption coefficient (α_{eff}) for the device TE_0 mode. In general, α_{eff} can be found via summation of absorption coefficients of all non-QD device layers weighted by their respective mode confinement factors. However, due to very low absorptivities of ZnO and TCTA at 630 nm (ref. 115 and ref. 116, respectively), optical losses are dominated by the L-ITO electrode ($\alpha_{L\text{-}ITO}$ = 161 cm^{-1})[28,117]. Therefore, α_{eff} can be estimated from $\alpha_{eff} \approx \Gamma_{L\text{-}ITO}\alpha_{L\text{-}ITO}$, which yields $\alpha_{eff} \approx 35$ cm^{-1}. This value is lower than the modal gain computed earlier, indicating the feasibility of lasing in the multi-layered LED-like device shown in Fig. 6a.

Indeed, the devices of ref. 28 showed good lasing performance under short-pulse optical excitation and exhibited single-mode lasing with a clear threshold at 65.6 μJ cm^{-2} (Fig. 6d). Importantly, the same structure, completed with a MoO_x/Al anode (Fig. 6b), also showed bright emission, under electrical excitation (Fig. 6e). This indicated that despite the QD layer was fairly thick by standards of traditional QD-LEDs, it could be efficiently excited by electric current. Another important observation was a high spatial uniformity of the emitted EL (inset of Fig. 6e), indicating that an underlying corrugation of an ITO electrode due to an integrated DFB resonator did not lead to either 'hot' or 'dead' injection spots. These results suggests that a properly designed QD structure can efficiently operate as both a lasing and an EL device, an important step towards a functional QLD.

While coming close to a true lasing action, the devices of ref. 28 did not lase under electrical pumping. One problem was an insufficient current density. Due to high resistivities of the L-ITO electrode and the thick QD layer, the devices experienced breakdown at j of ~0.2 A cm^{-2}, which was ~20 time lower than an estimated optical gain threshold. Another problem was quenching of a lasing mode by the top MoO_x/Al electrode. This is a known effect of metal contacts[118], which could be caused by reasons such as added optical losses (resulting from field penetration into a metal electrode), reduction of the field confinement factor for the active QD layer, and distortion of DFB cavity resonances.

None of the above hindrances, however, represent a fundamental obstacle which prohibits realization of QLDs. In particular, the problem of device breakdown can be resolved by methods such as 2D current focusing and short pulse electrical pumping, discussed earlier. There are also multiple approaches for tackling the problem of optical mode quenching induced by a metal electrode. For example, optical losses can be reduced by replacing a continuous metal film with a

mesh-like electrode[119] or a non-metal contact made of graphene[120] or a metal oxide[81]. Further, one can reduce optical-mode penetration into a charge-injecting contact by displacing it laterally versus a lasing region[121]. This suggests that the remaining roadblocks for the realization of QLDs can be removed in the near future, which will clear the path towards technologically viable lasing devices based on colloidal QDs.

Summary and outlook

There has been considerable effort across multiple disciplines directed towards the realization of electrically pumped lasers based on solution processable structures. This objective has been pursued using various material systems including semiconducting polymers[9,122], small molecules[98,123], carbon nanotubes[124,125], and perovskites prepared either as bulk films[126] or nanostructures with different form factors[127,128]. Colloidal QDs have been also part of this effort[13-15,26,28,99]. Starting with the first demonstration of ASE with these nanostructures[12], they have been investigated as active materials for colour-selectable lasers and optical amplifiers. This research has produced many important insights into photophysical properties of the QDs and, especially, behaviours of multi-carrier states that represent optical gain species in 0D materials.

Despite these advances, colloidal QD lasers are still at the stage of laboratory demonstrations. A primary challenge is extremely short lifetimes of gain-active multi-carrier states controlled by nonradiative Auger recombination[12,52]. This, in particular, greatly complicates the realization of lasing with cw optical and d.c. electrical excitation as the required excitation levels are too high to be withstood by colloidal nanomaterials[25,129]. As in the original demonstration of the ASE effect with colloidal nanocrystals[12], in most of the reported studies of QD lasing, this problem has been tackled using very short (sub-ps) high-intensity pump pulses typically derived from femtosecond

laser amplifiers. Such pump sources are complex and expensive, which greatly diminishes the practically utility of lasing devices based on colloidal nanostructures.

The situation, however, has recently changed due to the development of highly effective techniques for controlling Auger decay[26,47,73,78,130-132]. One such approach is based on the 'smoothing' of the confinement potential for supressing the intra-band transition involved in the dissipation of the e-h recombination energy[73]. The smooth potential profile can result, for example, from ionic inter-diffusion (intentional or unintentional) at a core/shell interface, as occurs, for example, during growth of thick-shell CdSe/CdS g-QDs[78,130]. It can be also realized using either 'discrete'[132] or 'continuous'[26,67] grading of a QD composition along a radial direction.

Lately, the 'grading approach' has been successfully implemented with CdSe/$Cd_xZn_{1-x}Se$-based cg-QDs[26,67]. These nanostructures demonstrate strong suppression of Auger decay, high emission rates, and large optical and electrical cross-sections. These properties have facilitated several important advances in the colloidal QD-LED and lasing fields, including the demonstration of low-threshold (sub-single-exciton) lasing using charged excitons as gain species[47], the realization of high-brightness, droop-free LEDs[67], and the attainment of optical gain with d.c. electrical pumping[26].

A recent result of most direct relevance to the QLD development, is the demonstration of cg-QD-based dual-function devices that operate as both an optically excited laser and a standard LED[28]. Due to insufficient stability at high *j*, these structures did not show lasing under electrical excitation. However, if combined with demonstrated schemes for achieving ultra-high current densities[99], the DFB-based architectures of ref. 28 should be capable of achieving the lasing regime. This suggests that all pieces of a QLD puzzle are finally in place, and electrically-pumped lasing with colloidal QDs may soon become a reality.

Acknowledgements

V.I.K and H.J were supported by the Laboratory Directed Research and Development (LDRD) program at Los Alamos National Laboratory under projects 20200213DR and 20210176ER, respectively. N.A. acknowledges support by a LANL Director's Postdoctoral Fellowship.

Additional information

Reprints and permissions information is available online at www.nature.com/reprints. Correspondence should be addressed to V.I.K.

Competing financial interests

The authors declare no competing financial interests.

FIGURES

Fig. 1| Electronic states in quantum dots (QDs) and principles of optical gain in QD media. **a,** Due to effects of 0D confinement, a QD exhibits discrete atomic-like states whose energies increase with decreasing QD size. As a result, the energy gap, E_g(QD), is a size dependent quantity. **b,** Size- and composition-tunable emission energies of QDs of IV-VI (PbS[34-36], PbSe[37], III-V (InP[32,33], and II-VI (CdE, E = Te[31,38], Se[17,29], S[30,38]) semiconductors (coloured symbols). Horizontal dashed lines of matching colours are the respective bulk-semiconductor energy gaps. **c,** A single-exciton QD state corresponds to optical transparency or optical gain threshold (middle). This regime corresponds to a transition from the 'absorbing' ground state (left) to the 'light-amplifying biexciton state (right). **d,** In QDs, light amplification due to stimulated emission from biexcitons (left) competes with biexciton decay via nonradiative Auger recombination (right).

Fig. 2| Principles of QD laser diodes (QLDs). a, A typical 'inverted' QD LED comprises an active QD layer sandwiched between electron and hole transport layers (ETL and HTL, respectively), supplemented by an ITO cathode and an Al/MoO_x anode. **b,** A QLD is an LED, which contains either an optical cavity for circulating light (red arrows) through a QD optical gain medium. **c,** A 'correlated' or 'sequential' charge injection model takes into consideration changes in the QD electrostatic (Coulomb) energy upon changes in the overall charge of the QD (ref. 26). In a standard LED, a QD is circulated between ground, $|0\rangle$, single-electron, $|e^-\rangle$, and single-exciton, $|X\rangle$, states ('blue cycle'). To realize a QLD, a QD must be circulated between $|X\rangle$, $|X^-\rangle$ (trion), and $|XX\rangle$ (biexciton) states ('red cycle'). τ_X, τ_{X^-} and τ_{XX} are the respective lifetimes, and g_e and g_h are the rates of electron and hole injection, respectively. Panel **a** is reproduced with permission from ref. 70. Springer Nature Limited.

Fig. 3| Three-state optical-gain model and gain media based on compositionally graded QDs (cg-QDs). a, A three-state model describes QD optical gain by transitions between $|0\rangle$, $|X\rangle$, and $|XX\rangle$ states whose occupation probabilities are P_0, P_X, and P_{XX}, respectively (ref. 42). **b,** In a QD emitting layer, organic ligands form an insulating membrane (blue), while QD semiconductor cores act as conducting channels (orange). This leads to 'current focusing' (black arrows), which increases a QD electrical cross-section (σ_e) compared to its geometric cross-section (σ_g). **c,** The band structure of a cg-QD, which comprises a CdSe core enclosed into a thick $Cd_xZn_{1-x}Se$ shell. **d,** Close-packed films of cg-QDs exhibit low-threshold random lasing under short-pulse excitation (100-fs, 3.1 eV pulses) at both band-edge (1S) and excited-state (1P) transitions[26]. Panel **a** is adapted with permission from ref. 42. ACS. Panels **c** and **d** are adapted with permission from ref. 26. Springer Nature Limited.

Fig. 4| Droop-free QD-LEDs enabled by QD- and device-level engineering. a, External quantum efficiency (EQE) versus current density (j) for an ideal 'droop-free' LED (green line) and a real-life device (red line) that exhibits EQE roll-off ('droop') at high j. EQE droop can be ascribed to nonradiative Auger recombination of charged excitons (right inset) that gradually replace neutral excitons (left inset) with increasing j. **b,** EQE-versus-luminance dependences for core/shell (C/S) 'ungraded' CdSe/$Cd_{0.7}Zn_{0.3}Se$ QDs (green squares) and similarly sized compositionally

graded CdSe/$Cd_xZn_{1-x}Se$ QDs without (blue circles) and with (red triangles) a final $ZnSe_yS_{1-y}$ 'barrier' shell (cg- and cg/B-QDs, respectively)[67]. The EQE droop can be evaluated in terms of j_{90}, the current density for which EQE is 90% of its peak value. For devices displayed in this figure, j_{90} = 861, 458, and 287 mA cm^{-2} (cg/B, cg, and C/S QDs, respectively). Panels **a** and **b** are adapted with permission from ref. 67. ACS.

Fig. 5| Optical gain using high-current-density QD-LEDs. a, An LED, which combines a current-focusing architecture (300×50 μm^2 active area) with pulsed electrical excitation, can achieve current densities (j) of ~1000 A cm^{-2}. **b, (Left)** j–V characteristics of a standard, "non-focusing" d.c. LED (black triangles) and a "current-focusing," pulsed LED (pulse duration τ_p = 1 μs; red circles) made of cg-QDs. For the first device, the maximal current density (j_{max}) is only ~3 A cm^{-2} at which point it experiences a breakdown ($V_{bd} \approx 14$ V). For the second device, V_{bd} is increased to 60 V and j_{max} to 1060 A cm^{-2}. **(Right)** Due to overheating of the active region, the electroluminescence (EL) spectrum shifts to lower energies with increasing V. Based on the measured shifts, the overheating (ΔT) at $V = V_{bd}$ is ~210 ºC for the standard device versus ~100 ºC for the current-focusing LED (estimated based on dE_g/dT = 0.28 meV per ºC; ref. 100). **c**, The EL spectra of the current-focusing LED for increasing j show a gradual increase in the relative intensity of the 1P versus the 1S feature, which indicates the increasing filling of the 1S level, followed by the filling of the 1P state. **d**, The analysis of the 1S- and 1 P-band intensities (symbols) using a 'correlated-injection' model of ref. 26 (lines) indicates that $\langle N \rangle$ reaches ca. 7 excitons per dot, which exceeds optical gain thresholds of both the 1S and 1P transitions ($\langle N_{th,gain} \rangle$ = 1.4 and 3.9, respectively)[26].

Fig. 6| A QD LED with an integrated optical cavity. a, An LED-like device that contains a second-order distributed feedback resonator (DFB) integrated into a bottom low-index ITO (L-ITO) electrode. **b,** A scanning electron microscopy image of a cg-QD-based laser/LED device demonstrated in ref. 28 (scale bar is 200 nm). **c**, The TE_0 optical mode profile for a device stack depicted in **a**. The mode confinement factors were computed for the 630 nm wavelength. **d,** Surface emission spectra of the device shown in **b** display a sharp transition to single-mode lasing at 65 μJ cm^{-2} (ref. 28) (excitation with 130-fs, 400-nm pump pulses). **e,** After this device is completed with a top contact, it exhibits spatially uniform EL (inset) peaked at 621 nm (ref. 28). **f,** EQE as a function of j indicates a peak efficiency of 4.3% (ref. 28). Due to high resistivity of the L-ITO electrode, the device exhibits a breakdown before it the optical gain regime (shaded area). Panels **a-f** are reproduced with permission from ref. 28. Springer Nature Limited.

REFERENCES

1 Hall, R. N., Carlson, R. O., Soltys, T. J., Fenner, G. E. & Kingsley, J. D. Coherent light emission from GaAs junctions. *Phys. Rev. Lett.* **9,** 366-368 (1962).

2 Nathan, M. I., Dumke, W. P., Burns, G., Dill, F. H. & Lasher, G. Stimulated emission of radiation from GaAs p-n junctions. *Appl. Phys. Lett.* **1,** 62-64 (1962).

3 Coldren, L. A., Corzine, S. W. & Mashanovitch, M. L. *Diode Lasers and Photonic Integrated Circuits, 2nd Ed.* (Wiley, Hoboken, 2012).

4 Holonyak, N., Kolbas, R., Dupuis, R. & Dapkus, P. Quantum-well heterostructure lasers. *IEEE J. Quantum Electron.* **16,** 170-186 (1980).

5 Jung, H. *et al.* Efficient on-chip integration of a colloidal quantum dot photonic crystal band-edge laser with a coplanar waveguide. *Opt. Express* **25,** 32919-32930 (2017).

6 Clark, J. & Lanzani, G. Organic photonics for communications. *Nature Photon.* **4,** 438-446 (2010).

7 Xie, W. *et al.* On-chip integrated quantum-dot–silicon-nitride microdisk lasers. *Adv. Mater.* **29,** 1604866 (2017).

8 Cegielski, P. J. *et al.* Monolithically integrated perovskite semiconductor lasers on silicon photonic chips by scalable top-down fabrication. *Nano Lett.* **18,** 6915-6923 (2018).

9 Karl, M. *et al.* Flexible and ultra-lightweight polymer membrane lasers. *Nature Commun.* **9,** 1525 (2018).

10 Vannahme, C., Klinkhammer, S., Lemmer, U. & Mappes, T. Plastic lab-on-a-chip for fluorescence excitation with integrated organic semiconductor lasers. *Opt. Express* **19,** 8179-8186 (2011).

11 Chen, Y.-C. & Fan, X. Biological lasers for biomedical applications. *Adv. Opt. Mater.* **7,** 1900377 (2019).

12 Klimov, V. I. *et al.* Optical gain and stimulated emission in nanocrystal quantum dots. *Science* **290,** 314-317 (2000).

13 Wang, Y. & Sun, H. Advances and prospects of lasers developed from colloidal semiconductor nanostructures. *Prog. Quantum Electron.* **60,** 1-29 (2018).

14 Geiregat, P., Van Thourhout, D. & Hens, Z. A bright future for colloidal quantum dot lasers. *NPG Asia Mater.* **11,** 41 (2019).

15 Park, Y.-S., Roh, J., Diroll, B. T., Schaller, R. D. & Klimov, V. I. Colloidal quantum dot lasers. *Nature Rev. Mater.* (2021).

16 Peng, X., Schlamp, M. C., Kadavanich, A. V. & Alivisatos, A. P. Epitaxial growth of highly luminescent CdSe/CdS core/shell nanocrystals with photostability and electronic accessibility. *J. Am. Chem. Soc.* **119,** 7019-7029 (1997).

17 Murray, C. B., Norris, D. J. & Bawendi, M. G. Synthesis and characterization of nearly monodisperse CdE (E = sulfur, selenium, tellurium) semiconductor nanocrystallites. *J. Am. Chem. Soc.* **115,** 8706-8715 (1993).

18 Peng, X. *et al.* Shape control of CdSe nanocrystals. *Nature* **404,** 59-61 (2000).

19 Li, L.-s., Walda, J., Manna, L. & Alivisatos, A. P. Semiconductor nanorod liquid crystals. *Nano Lett.* **2,** 557-560 (2002).

20 Manna, L., Milliron, D. J., Meisel, A., Scher, E. C. & Alivisatos, A. P. Controlled growth of tetrapod-branched inorganic nanocrystals. *Nature Mater.* **2,** 382-385 (2003).
21 Joo, J., Son, J. S., Kwon, S. G., Yu, J. H. & Hyeon, T. Low-temperature solution-phase synthesis of quantum well structured CdSe nanoribbons. *J. Am. Chem. Soc.* **128,** 5632-5633 (2006).
22 Ithurria, S. *et al.* Colloidal nanoplatelets with two-dimensional electronic structure. *Nature Mater.* **10,** 936-941 (2011).
23 Hines, M. A. & Guyot-Sionnest, P. Synthesis and characterization of strongly luminescing ZnS-capped CdSe nanocrystals. *J. Phys. Chem.* **100,** 468-471 (1996).
24 Pietryga, J. M. *et al.* Spectroscopic and device aspects of nanocrystal quantum dots. *Chem. Rev.* **116,** 10513-10622 (2016).
25 Fan, F. *et al.* Continuous-wave lasing in colloidal quantum dot solids enabled by facet-selective epitaxy. *Nature* **544,** 75-79 (2017).
26 Lim, J., Park, Y.-S. & Klimov, V. I. Optical gain in colloidal quantum dots achieved with direct-current electrical pumping. *Nature Mater.* **17,** 42-49 (2018).
27 Xie, W. *et al.* On-chip integrated quantum-dot-silicon-nitride microdisk lasers. *Adv. Mater.* **29,** 1604866 (2017).
28 Roh, J., Park, Y.-S., Lim, J. & Klimov, V. I. Optically pumped colloidal-quantum-dot lasing in LED-like devices with an integrated optical cavity. *Nature Commun.* **11,** 271 (2020).
29 Peng, X., Wickham, J. & Alivisatos, A. P. Kinetics of II-VI and III-V colloidal semiconductor nanocrystal growth: "focusing" of size distributions. *J. Am. Chem. Soc.* **120,** 5343-5344 (1998).
30 Yu, W. W. & Peng, X. Formation of high-quality CdS and other II-VI semiconductor nanocrystals in noncoordinating solvents: tunable reactivity of monomers. *Angew. Chem. Int. Ed.* **41,** 2368-2371 (2002).
31 Yu, W. W., Wang, Y. A. & Peng, X. Formation and stability of size-, shape-, and structure-controlled CdTe nanocrystals: ligand effects on monomers and nanocrystals. *Chem. Mater.* **15,** 4300-4308 (2003).
32 Biadala, L. *et al.* Band-edge exciton fine structure and recombination dynamics in InP/ZnS colloidal nanocrystals. *ACS Nano* **10,** 3356-3364 (2016).
33 Mićić, O. I. *et al.* Size-dependent spectroscopy of InP quantum dots. *J. Phys. Chem. B* **101,** 4904-4912 (1997).
34 Sun, L. *et al.* Bright infrared quantum-dot light-emitting diodes through inter-dot spacing control. *Nature Nanotech.* **7,** 369-373 (2012).
35 Moreels, I. *et al.* Size-dependent optical properties of colloidal PbS quantum dots. *ACS Nano* **3,** 3023-3030 (2009).
36 Miller, E. M. *et al.* Revisiting the valence and conduction band size dependence of PbS quantum dot thin films. *ACS Nano* **10,** 3302-3311 (2016).
37 Pietryga, J. M. *et al.* Pushing the band gap envelope: mid-infrared emitting colloidal PbSe quantum dots. *J. Am. Chem. Soc.* **126,** 11752-11753 (2004).
38 Yu, W. W., Qu, L., Guo, W. & Peng, X. Experimental determination of the extinction coefficient of CdTe, CdSe, and CdS nanocrystals. *Chem. Mater.* **15,** 2854-2860 (2003).
39 Arakawa, Y. & Sakaki, H. Multidimensional quantum well laser and temperature dependence of its threshold current. *Appl. Phys. Lett.* **40,** 939-941 (1982).

40 Asada, M., Miyamoto, Y. & Suematsu, Y. Gain and the threshold of three-dimensional quantum-box lasers. *IEEE J. Quantum Electron.* **22,** 1915-1921 (1986).
41 Moreels, I. *et al.* Nearly temperature-independent threshold for amplified spontaneous emission in colloidal CdSe/CdS quantum dot-in-rods. *Adv. Mater.* **24**, OP231-OP235 (2012).
42 Park, Y.-S., Bae, W. K., Baker, T., Lim, J. & Klimov, V. I. Effect of Auger recombination on lasing in heterostructured quantum dots with engineered core/shell interfaces. *Nano Lett.* **15,** 7319-7328 (2015).
43 Schaller, R. D., Petruska, M. A. & Klimov, V. I. Tunable near-infrared optical gain and amplified spontaneous emission using PbSe nanocrystals. *J. Phys. Chem. B* **107**, 13765-13768 (2003).
44 Klimov, V. I. *et al.* Single-exciton optical gain in semiconductor nanocrystals. *Nature* **447**, 441-446 (2007).
45 Wu, K., Park, Y.-S., Lim, J. & Klimov, V. I. Towards zero-threshold optical gain using charged semiconductor quantum dots. *Nature Nanotech.* **12,** 1140-1147 (2017).
46 Wang, C., Wehrenberg, B. L., Woo, C. Y. & Guyot-Sionnest, P. Light emission and amplification in charged CdSe quantum dots. *J. Phys. Chem. B* **108**, 9027-9031 (2004).
47 Kozlov, O. V. *et al.* Sub–single-exciton lasing using charged quantum dots coupled to a distributed feedback cavity. *Science* **365,** 672-675 (2019).
48 Yu, J. *et al.* Electrically control amplified spontaneous emission in colloidal quantum dots. *Sci. Adv.* **5**, eaav3140 (2019).
49 Christodoulou, S. *et al.* Single-exciton gain and stimulated emission across the infrared telecom band from robust heavily doped PbS colloidal quantum dots. *Nano Lett.* **20**, 5909-5915 (2020).
50 Landsberg, P. T. *Recombination in Semiconductors* (Cambridge Univ. Press, Cambridge, 1991).
51 Pietryga, J. M., Zhuravlev, K. K., Whitehead, M., Klimov, V. I. & Schaller, R. D. Evidence for barrierless Auger recombination in PbSe nanocrystals: a pressure-dependent study of transient optical absorption. *Phys. Rev. Lett.* **101,** 217401 (2008).
52 Klimov, V. I., Mikhailovsky, A. A., McBranch, D. W., Leatherdale, C. A. & Bawendi, M. G. Quantization of multiparticle Auger rates in semiconductor quantum dots. *Science* **287,** 1011-1013 (2000).
53 Robel, I., Gresback, R., Kortshagen, U., Schaller, R. D. & Klimov, V. I. Universal size-dependent trend in Auger recombination in direct-gap and indirect-gap semiconductor nanocrystals. *Phys. Rev. Lett.* **102,** 177404 (2009).
54 Crooker, S. A., Barrick, T., Hollingsworth, J. A. & Klimov, V. I. Multiple temperature regimes of radiative decay in CdSe nanocrystal quantum dots: intrinsic lmits of the dark-exciton lifetime. *Appl. Phys. Lett.* **82,** 2793-2795 (2003).
55 Klimov, V. I. Multicarrier interactions in semiconductor nanocrystals in relation to the phenomena of Auger recombination and carrier multiplication. *Annu. Rev. Cond. Matt. Phys.* **5,** 285-316 (2014).
56 Mikhailovsky, A. A., Malko, A. V., Hollingsworth, J. A., Bawendi, M. G. & Klimov, V. I. Multiparticle interactions and stimulated emission in chemically synthesized quantum dots. *Appl. Phys. Lett.* **80,** 2380-2382 (2002).

57 Eisler, H.-J. *et al.* Color-selective semiconductor nanocrystal laser. *Appl. Phys. Lett.* **80,** 4614-4616 (2002).
58 Malko, A. V. *et al.* From amplified spontaneous emission to microring lasing using nanocrystal quantum dot solids. *Appl. Phys. Lett.* **81,** 1303-1305 (2002).
59 Dang, C. *et al.* Red, green and blue lasing enabled by single-exciton gain in colloidal quantum dot films. *Nature Nanotech.* **7**, 335-339 (2012).
60 Kazes, M., Lewis, D. Y., Ebenstein, Y., Mokari, T. & Banin, U. Lasing from semiconductor quantum rods in a cylindrical microcavity. *Adv. Mater.* **14,** 317-321 (2002).
61 Zavelani-Rossi, M., Lupo, M. G., Krahne, R., Manna, L. & Lanzani, G. J. N. Lasing in self-assembled microcavities of CdSe/CdS core/shell colloidal quantum rods. *Nanoscale* **2,** 931-935 (2010).
62 She, C. *et al.* Red, yellow, green, and blue amplified spontaneous emission and lasing using colloidal CdSe nanoplatelets. *ACS Nano* **9,** 9475-9485 (2015).
63 Grim, J. Q. *et al.* Continuous-wave biexciton lasing at room temperature using solution-processed quantum wells. *Nature Nanotech.* **9**, 891-895 (2014).
64 Yakunin, S. *et al.* Low-threshold amplified spontaneous emission and lasing from colloidal nanocrystals of caesium lead halide perovskites. *Nature Commun.* **6,** 8056 (2015).
65 Shirasaki, Y., Supran, G. J., Bawendi, M. G. & Bulovic, V. Emergence of colloidal quantum-dot light-emitting technologies. *Nature Photon.* **7,** 13-23 (2013).
66 Dai, X. *et al.* Solution-processed, high-performance light-emitting diodes based on quantum dots. *Nature* **515,** 96-99 (2014).
67 Lim, J., Park, Y.-S., Wu, K., Yun, H. J. & Klimov, V. I. Droop-free colloidal quantum dot light-emitting diodes. *Nano Lett.* **18,** 6645-6653 (2018).
68 Li, X. *et al.* Bright colloidal quantum dot light-emitting diodes enabled by efficient chlorination. *Nature Photon.* **12,** 159-164 (2018).
69 Sun, Y. *et al.* Investigation on thermally induced efficiency roll-off: toward efficient and ultrabright quantum-dot light-emitting diodes. *ACS Nano* **13,** 11433-11442 (2019).
70 Bae, W. K. *et al.* Controlling the influence of Auger recombination on the performance of quantum-dot light-emitting diodes. *Nature Commun.* **4,** 3661 (2013).
71 Garcia-Santamaria, F. *et al.* Suppressed Auger recombination in "giant" nanocrystals boosts optical gain performance. *Nano Lett.* **9,** 3482-3488 (2009).
72 Bisschop, S., Geiregat, P., Aubert, T. & Hens, Z. The impact of core/shell sizes on the optical gain characteristics of CdSe/CdS quantum dots. *ACS Nano* **12,** 9011-9021 (2018).
73 Cragg, G. E. & Efros, A. L. Suppression of Auger processes in confined structures. *Nano Lett.* **10**, 313-317 (2010).
74 Vaxenburg, R., Lifshitz, E. & Efros, A. L. Suppression of Auger-stimulated efficiency droop in nitride-based light emitting diodes. *Appl. Phys. Lett.* **102,** 031120 (2013).
75 Klimov, V. I., McGuire, J. A., Schaller, R. D. & Rupasov, V. I. Scaling of multiexciton lifetimes in semiconductor nanocrystals. *Phys. Rev. B* **77**, 195324 (2008).
76 Achermann, M., Bartko, A. P., Hollingsworth, J. A. & Klimov, V. I. The effect of Auger heating on intraband carrier relaxation in semiconductor qauntum dots. *Nature Phys.* **2,** 557-561 (2006).

77 Zhang, M., Bhattacharya, P., Singh, J. & Hinckley, J. Direct measurement of auger recombination in $In_{0.1}Ga_{0.9}N$/GaN quantum wells and its impact on the efficiency of $In_{0.1}Ga_{0.9}N$/GaN multiple quantum well light emitting diodes. *Appl. Phys. Lett.* **95**, 201108 (2009).
78 Bae, W. K. *et al.* Controlled alloying of the core–shell interface in CdSe/CdS quantum dots for suppression of Auger recombination. *ACS Nano* **7,** 3411-3419 (2013).
79 Kwak, J. *et al.* Bright and efficient full-color colloidal quantum dot light-emitting diodes using an inverted device structure. *Nano Lett.* **12,** 2362-2366 (2012).
80 Shahnawaz, S. *et al.* Hole-transporting materials for organic light-emitting diodes: an overview. *J. Mater. Chem. C* **7,** 7144-7158 (2019).
81 Choi, M. K. *et al.* Extremely vivid, highly transparent, and ultrathin quantum dot light-emitting diodes. *Adv. Mater.* **30,** 1703279 (2018).
82 Kim, H.-M., Cho, S., Kim, J., Shin, H. & Jang, J. Li and Mg co-doped zinc oxide electron transporting layer for highly efficient quantum dot light-emitting diodes. *ACS Appl. Mater. Interfaces* **10,** 24028-24036 (2018).
83 Nam, S., Oh, N., Zhai, Y. & Shim, M. High efficiency and optical anisotropy in double-heterojunction nanorod light-emitting diodes. *ACS Nano* **9,** 878-885 (2015).
84 Rhee, S. *et al.* "Positive incentive" approach to enhance the operational stability of quantum dot-based light-emitting diodes. *ACS Appl. Mater. Interfaces* **11,** 40252-40259 (2019).
85 Moon, H. & Chae, H. Efficiency enhancement of all-solution-processed inverted-structure green quantum dot light-emitting diodes via partial ligand exchange with thiophenol derivatives having negative dipole moment. *Adv. Opt. Mater.* **8,** 1901314 (2019).
86 Bruening, M. *et al.* Polar Ligand adsorption controls semiconductor surface potentials. *J. Am. Chem. Soc.* **116**, 2972-2977 (1994).
87 Zhao, Y. *et al.* High-temperature luminescence quenching of colloidal quantum dots. *ACS Nano* **6,** 9058-9067 (2012).
88 Rowland, C. E. *et al.* Thermal stability of colloidal InP nanocrystals: small inorganic ligands boost high-temperature photoluminescence. *ACS Nano* **8,** 977-985 (2013).
89 Panda, S. K., Hickey, S. G., Waurisch, C. & Eychmüller, A. Gradated alloyed CdZnSe nanocrystals with high luminescence quantum yields and stability for optoelectronic and biological applications. *J. Mater. Chem.* **21,** 11550-11555 (2011).
90 Bae, W. K., Nam, M. K., Char, K. & Lee, S. Gram-scale one-pot synthesis of highly luminescent blue emitting $Cd_{1-x}Zn_xS$/ZnS nanocrystals. *Chem. Mater.* **20,** 5307-5313 (2008).
91 Tokito, S., Tanaka, H., Noda, K., Okada, A. & Taga, Y. Thermal stability in oligomeric triphenylamine/tris(8-quinolinolato) aluminum electroluminescent devices. *Appl. Phys. Lett.* **70,** 1929-1931 (1997).
92 Fenter, P., Schreiber, F., Bulović, V. & Forrest, S. R. Thermally induced failure mechanisms of organic light emitting device structures probed by X-ray specular reflectivity. *Chem. Phys. Lett.* **277,** 521-526 (1997).
93 Lee, J. B. & Subramanian, V. Weave patterned organic transistors on fiber for E-textiles. *IEEE Trans. Electron Devices* **52,** 269-275 (2005).

94 Azrain, M. M., Omar, G., Mansor, M. R., Fadzullah, S. H. S. M. & Lim, L. M. Failure mechanism of organic light emitting diodes (OLEDs) induced by hygrothermal effect. *Opt. Mater.* **91,** 85-92 (2019).
95 Talapin, D. V., Murray, C. B. PbSe nanocrystal solids for n- and p-channel thin film field-effect transistors. *Science* **310**, 86-89 (2005).
96 Wang, R. *et al.* Colloidal quantum dot ligand engineering for high performance solar cells. *Energy Environ. Sci.* **9**, 1130-1143 (2016).
97 Kim, H. *et al.* Hybrid perovskite light emitting diodes under intense electrical excitation. *Nature Commun.* **9,** 4893 (2018).
98 Sandanayaka, A. S. D. *et al.* Indication of current-injection lasing from an organic semiconductor. *Appl. Phys. Express* **12,** 061010 (2019).
99 Jung, H., Park, Y.-S., Lim, J., Fedin, I. & Klimov, V. I. Complete population inversion of 1S and 1P transitions in colloidal quantum dots driven by ultra-high current densities of more than 1,000 A per cm^2. Unpublished (2021).
100 Albahrani, S. M. B. *et al.* Quantum dots to probe temperature and pressure in highly confined liquids. *RSC Adv.* **8,** 22897-22908 (2018).
101 Lu, C.-Y., Chang, S.-W., Chuang, S. L., Germann, T. D. & Bimberg, D. Metal-cavity surface-emitting microlaser at room temperature. *Appl. Phys. Lett.* **96,** 251101 (2010).
102 Tischler, J. R., Bradley, M. S., Bulović, V., Song, J. H. & Nurmikko, A. Strong coupling in a microcavity LED. *Phys. Rev. Lett.* **95,** 036401 (2005).
103 Tawara, T., Gotoh, H., Akasaka, T., Kobayashi, N. & Saitoh, T. Low-threshold lasing of InGaN vertical-cavity surface-emitting lasers with dielectric distributed Bragg reflectors. *Appl. Phys. Lett.* **83,** 830-832 (2003).
104 Wang, L. *et al.* Red, green, and blue microcavity quantum dot light-emitting devices with narrow line widths. *ACS Appl. Nano Mater.* **3,** 5301-5310 (2020).
105 Nakamura, S. *et al.* InGaN multi-quantum-well-structure laser diodes with cleaved mirror cavity facets. *Jpn. J. Appl. Phys.* **35,** L217-L220 (1996).
106 Bulman, G. E. *et al.* Pulsed operation lasing in a cleaved-facet InGaN/GaN MQW SCH laser grown on 6H-SiC. *Electron. Lett.* **33,** 1556-1557 (1997).
107 McGehee, M. D. & Heeger, A. J. Semiconducting (conjugated) polymers as materials for solid-state lasers. *Adv. Mater.* **12,** 1655-1668 (2000).
108 Fu, Y. & Zhai, T. Distributed feedback organic lasing in photonic crystals. *Front. Optoelectron.* **13,** 18-34 (2020).
109 Shyh, W. Principles of distributed feedback and distributed Bragg-reflector lasers. *IEEE J. Quantum Electron.* **10,** 413-427 (1974).
110 Karnutsch, C. *et al.* Low threshold blue conjugated polymer lasers with first- and second-order distributed feedback. *Appl. Phys. Lett.* **89,** 201108 (2006).
111 Bjorkholm, J. E. & Shank, C. V. Higher-order distributed feedback oscillators. *Appl. Phys. Lett.* **20,** 306-308 (1972).
112 Henry, C., Kazarinov, R., Logan, R. & Yen, R. Observation of destructive interference in the radiation loss of second-order distributed feedback lasers. *IEEE J. Quantum Electron.* **21,** 151-154 (1985).
113 Dang, C. *et al.* Highly efficient, spatially coherent distributed feedback lasers from dense colloidal quantum dot films. *Appl. Phys. Lett.* **103,** 171104 (2013).

114 Signorini, R. *et al.* Facile production of up-converted quantum dot lasers. *Nanoscale* **3,** 4109-4113 (2011).
115 Amakali, T., Daniel, L. S., Uahengo, V., Dzade, N. Y. & de Leeuw, N. H. Structural and optical properties of ZnO thin films prepared by molecular precursor and sol–gel methods. *Crystals* **10,** 132 (2020).
116 Kim, H.-B. & Kim, J.-J. Diffusion mechanism of exciplexes in organic optoelectronics. *Phys. Rev. Appl.* **13,** 024006 (2020).
117 Moerland, R. J. & Hoogenboom, J. P. Subnanometer-accuracy optical distance ruler based on fluorescence quenching by transparent conductors. *Optica* **3,** 112-117 (2016).
118 Reufer, M. *et al.* Low-threshold polymeric distributed feedback lasers with metallic contacts. *Appl. Phys. Lett.* **84,** 3262-3264 (2004).
119 Jing, P. *et al.* Vacuum-free transparent quantum dot light-emitting diodes with silver nanowire cathode. *Sci. Rep.* **5,** 12499 (2015).
120 Seo, J.-T. *et al.* Fully transparent quantum dot light-emitting diode integrated with graphene anode and cathode. *ACS Nano* **8,** 12476-12482 (2014).
121 Shayesteh, M. R. Design and analysis of an electrically pumped microcavity organic laser device. *Electron. Mater. Lett.* **13,** 207-213 (2017).
122 Tessler, N., Denton, G. J. & Friend, R. H. Lasing from conjugated-polymer microcavities. *Nature* **382,** 695-697 (1996).
123 Kozlov, V. G., Bulović, V., Burrows, P. E. & Forrest, S. R. Laser action in organic semiconductor waveguide and double-heterostructure devices. *Nature* **389,** 362-364 (1997).
124 Gaufrès, E. *et al.* Optical gain in carbon nanotubes. *Appl. Phys. Lett.* **96,** 231105 (2010).
125 Graf, A. *et al.* Electrical pumping and tuning of exciton-polaritons in carbon nanotube microcavities. *Nature Mater.* **16,** 911-917 (2017).
126 Saliba, M. *et al.* Structured organic-inorganic perovskite toward a distributed feedback laser. *Adv. Mater.* **28,** 923-929 (2016).
127 Jia, Y., Kerner, R. A., Grede, A. J., Rand, B. P. & Giebink, N. C. Continuous-wave lasing in an organic–inorganic lead halide perovskite semiconductor. *Nature Photon.* **11,** 784-788 (2017).
128 Wang, Y.-C. *et al.* Flexible organometal–halide perovskite lasers for speckle reduction in imaging projection. *ACS Nano* **13,** 5421-5429 (2019).
129 Adachi, M. M. *et al.* Microsecond-sustained lasing from colloidal quantum dot solids. *Nature Commun.* **6,** 8694 (2015).
130 Garcia-Santamaria, F. *et al.* Breakdown of volume scaling in Auger recombination in CdSe/CdS heteronanocrystals: the role of the core-shell interface. *Nano Lett.* **11,** 687-693 (2011).
131 Nasilowski, M., Spinicelli, P., Patriarche, G. & Dubertret, B. Gradient CdSe/CdS quantum dots with room temperature biexciton unity quantum yield. *Nano Lett.* **15**, 3953-3958 (2015).
132 Park, Y.-S., Lim, J., Makarov, N. S. & Klimov, V. I. Effect of interfacial alloying versus “volume scaling” on Auger recombination in compositionally graded semiconductor quantum dots. *Nano Lett.* **17,** 5607-5613 (2017).

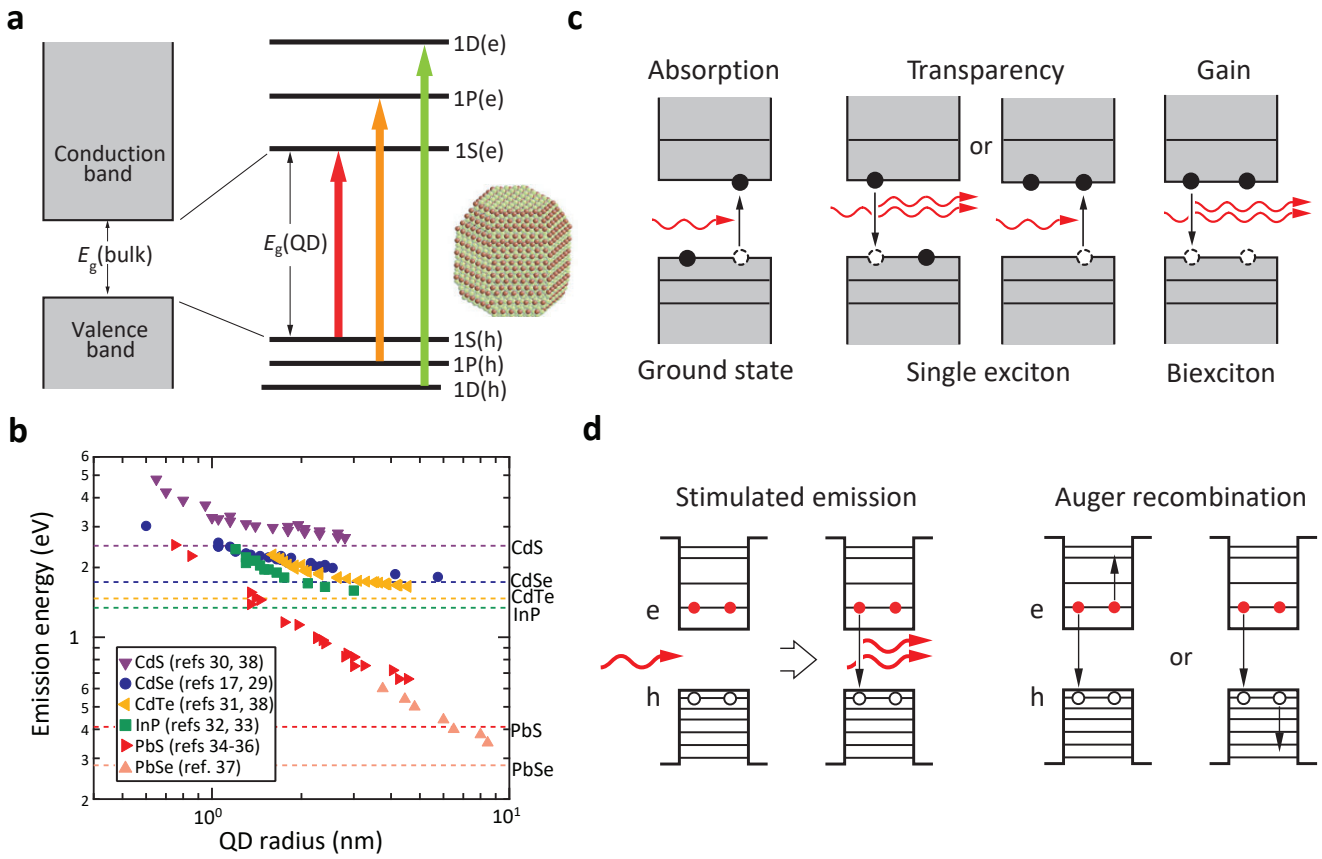

Fig. 1| Electronic states in quantum dots (QDs) and principles of optical gain and lasing in QD media

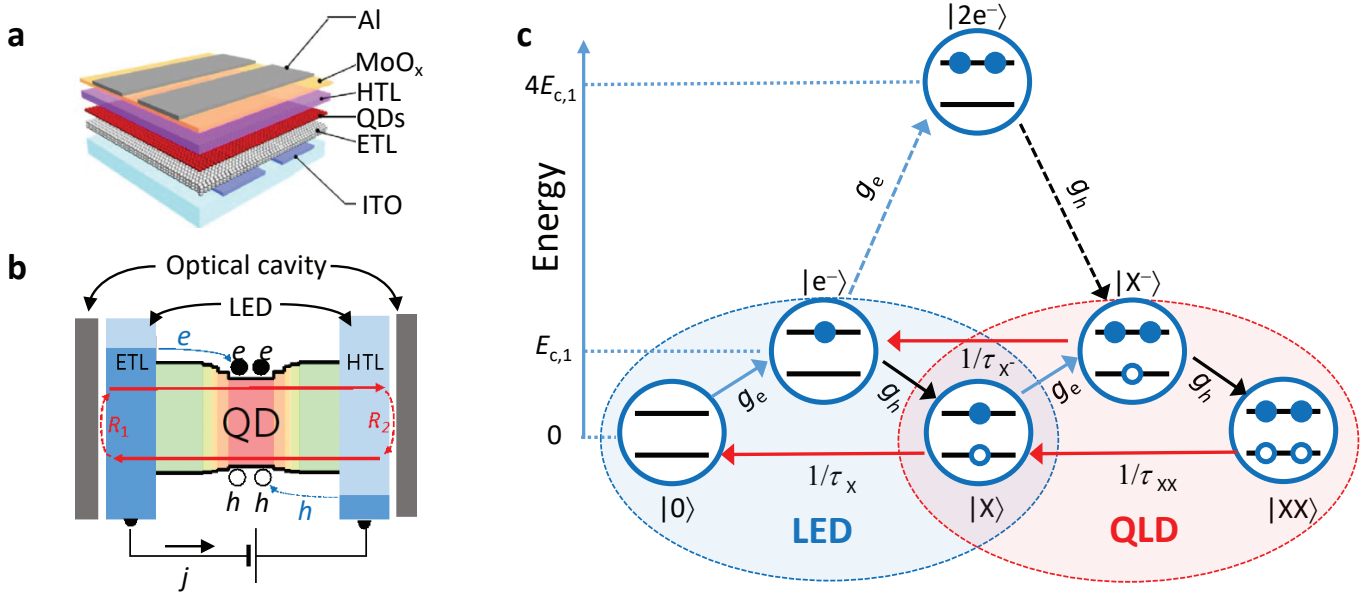

Fig. 2| Principles of QD laser diodes (QLDs) and a QLD charge-injection model

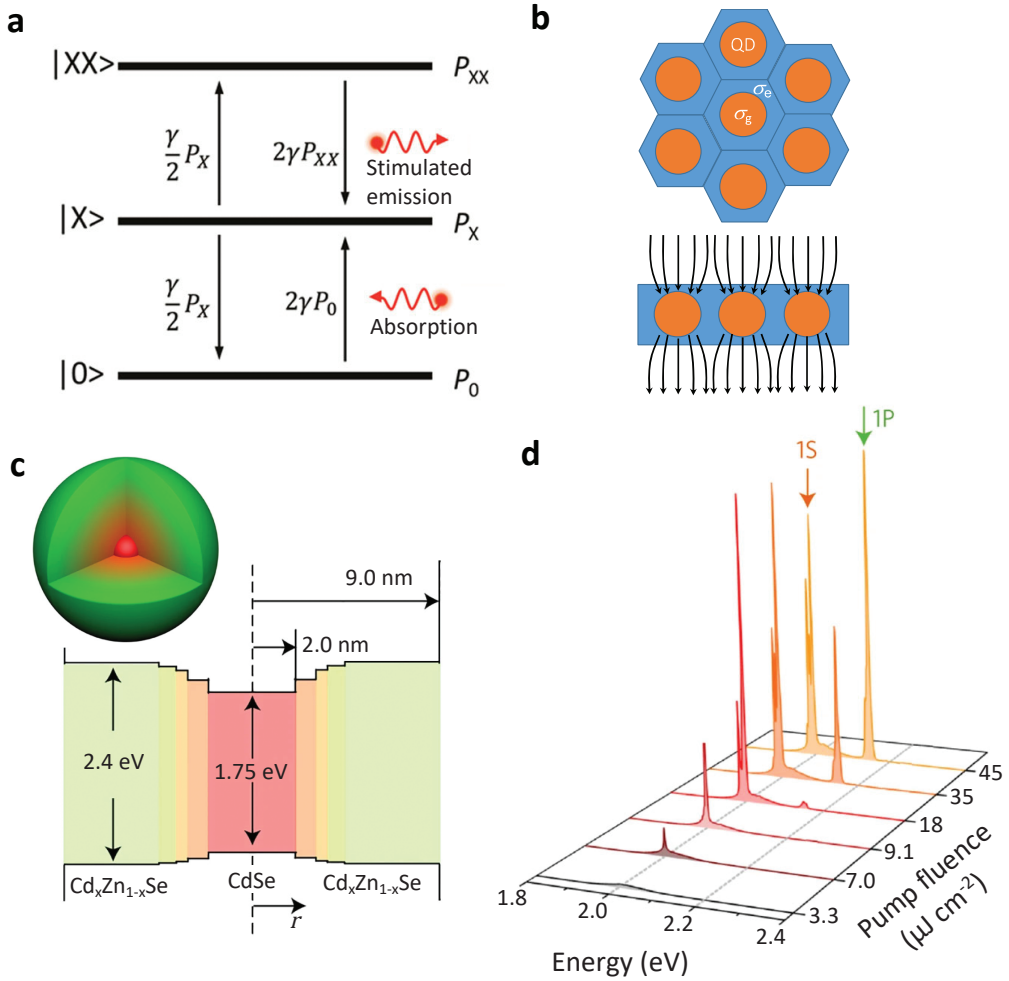

Fig. 3| Optical gain model and control of gain-related QD properties

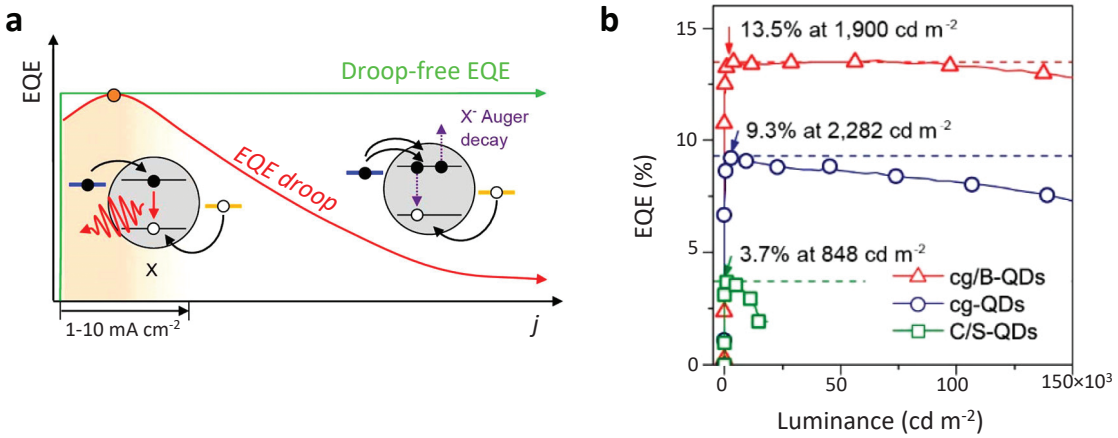

Fig. 4| Droop-free QD-LEDs enabled by QD- and device-level engineering

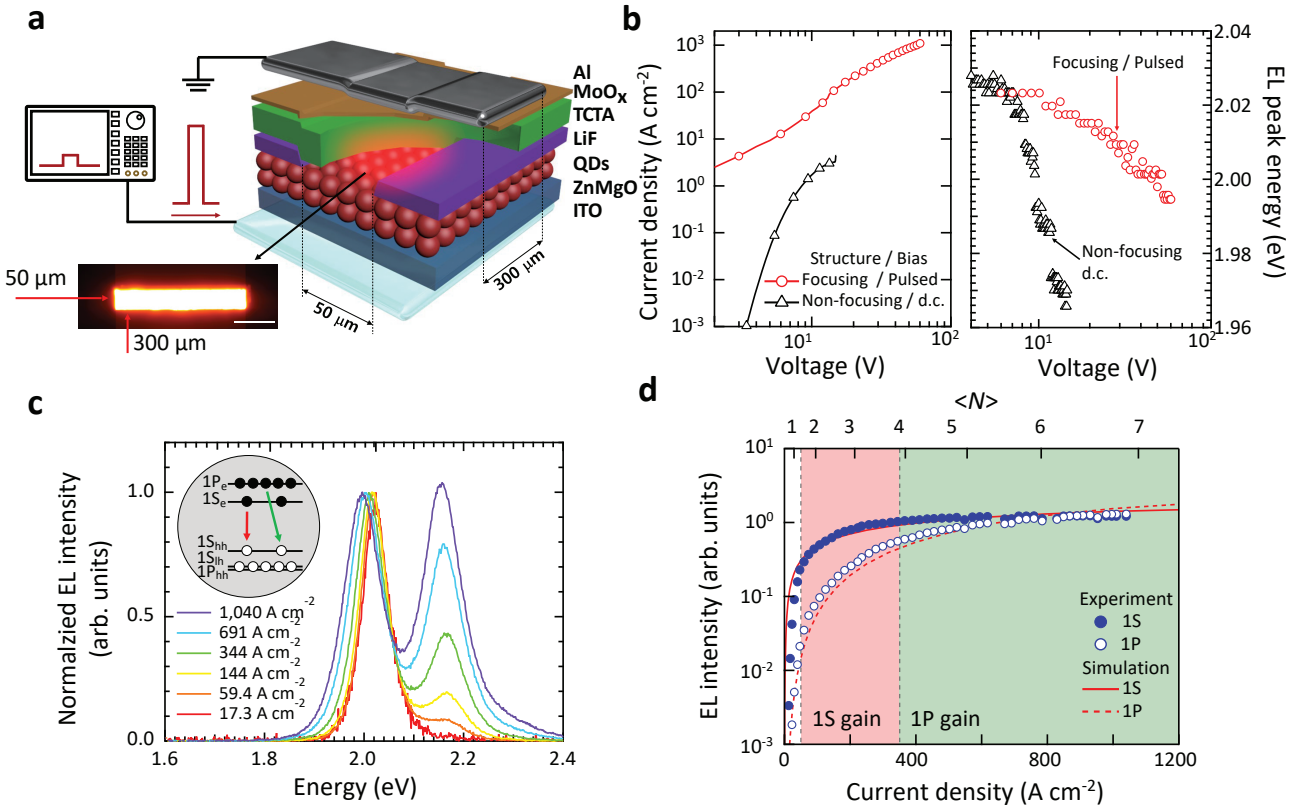

Fig. 5| Realization of optical gain in high-current-density QD-LEDs

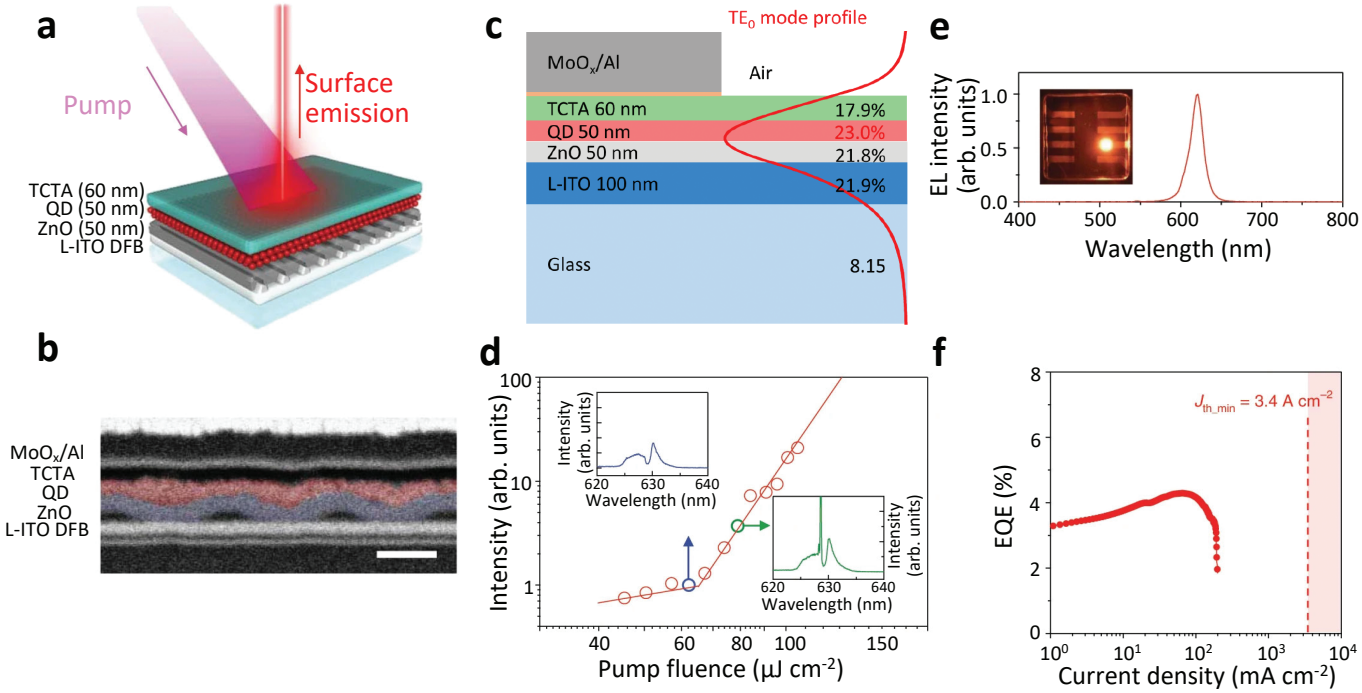

Fig. 6| Integration of an optical cavity into a QD electroluminescent device